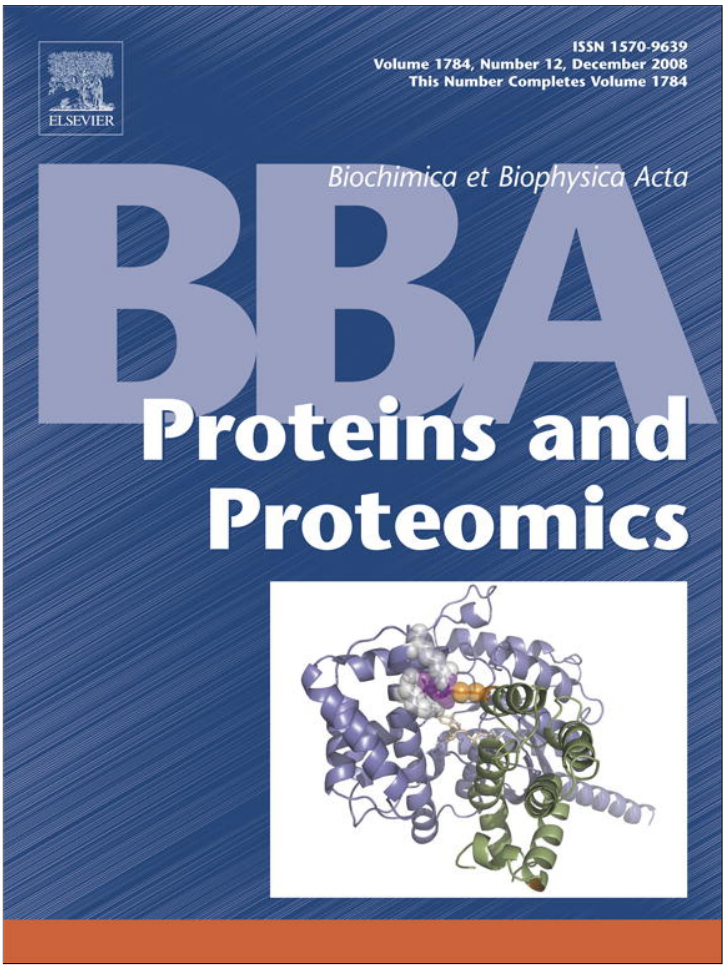

Biochimica et Biophysica Acta 1784 (2008) 1924–1934

Contents lists available at ScienceDirect

Biochimica et Biophysica Acta

journal homepage: www.elsevier.com/locate/bbapap

The family 52 β-xylosidase from *Geobacillus stearothermophilus* is a dimer: Structural and biophysical characterization of a glycoside hydrolase

Lellys M. Contreras [a,*,1], Javier Gómez [b], Jesús Prieto [c], Josefa M. Clemente-Jiménez [d], Francisco J. Las Heras-Vázquez [d], Felipe Rodríguez-Vico [d], Francisco J. Blanco [e], José L. Neira [b,f,*]

[a] *Departamento de Biología, Facultad Experimental de Ciencias y Tecnología, Universidad de Carabobo, 2001 Valencia, Venezuela*
[b] *Instituto de Biología Molecular y Celular, Universidad Miguel Hernández, 03202 Elche (Alicante), Spain*
[c] *Structural Biology and Biocomputing Programme, Centro Nacional de Investigaciones Oncológicas (CNIO), 28007 Madrid, Spain*
[d] *Departamento de Química Física, Bioquímica y Química Inorgánica, Universidad de Almería, 04120 Almería, Spain*
[e] *Structural Biology Unit, CIC bioGUNE, Ed. 801A, Parque Tecnológico de Bizkaia, 48160 Derio (Vizcaya), Spain*
[f] *Biocomputation and Complex Systems Physics Institute, 50009 Zaragoza, Spain*

ARTICLE INFO

Article history:
Received 29 April 2008
Received in revised form 24 June 2008
Accepted 25 June 2008
Available online 8 July 2008

Keywords:
Conformation
FTIR
Molten globule
Fluorescence
Circular dichroism
Structure

ABSTRACT

Xylans are the most abundant polysaccharides forming the plant cell wall hemicelluloses, and they are degraded, among other proteins, by β-xylosidase enzymes. In this work, the structural and biophysical properties of the family 52 β-xylosidase from *Geobacillus stearothermophilus*, XynB2, are described. Size exclusion chromatography, analytical centrifugation, ITC, CD, fluorescence (steady state and ANS-binding) and FTIR were used to obtain the structure, the oligomerization state and the conformational changes of XynB2, as pH, chemical denaturants or temperature were modified. This report describes the first extensive conformational characterization of a family 52 β-xylosidase. The active protein was a highly hydrated dimer, whose active site was formed by the two protomers, and it probably involved aromatic residues. At low pH, the protein was not active and it populated a monomeric molten-globule-like species, which had a conformational transition with a pK_a of ~4.0. Thermal and chemical-denaturations of the native protein showed hysteresis behaviour. The protein at physiological pH was formed by α-helix (30%) and β-sheet (30%), as shown by CD and FTIR. Comparison with other xylosidases of the same family indicates that the percentages of secondary structure seem to be conserved among the members of the family.

1. Introduction

Sugars have important roles in energy storage, specific molecular recognition, and in defining the structural framework of cells [1–5]. In addition, carbohydrates are important in several biotechnological applications, such as baking and paper bleaching [6–8]. However, efficient synthetic methods for the large-scale production, purification and use of saccharides are currently unavailable, due to the need of protecting specific hydroxyl groups to obtain well-defined products. For this reason, enzyme synthesis of sugars is an alternative to classic synthetic methods: enzymes are highly specific and allow the formation of newly generated anomeric sites.

Xylans are the most abundant polysaccharides constitutive of plant cell wall hemicelluloses, and the second most abundant sugars in Nature. They are formed by a backbone of β-1,4-linked xylopyranosyl units carrying various substituents such as arabinofuranose, glucuronic acid, methylglucoronic acid and acetyl groups [9]. Thus, complete degradation of xylan requires the action of several hydrolytic enzymes [10]. These xylan-degrading enzymes include among others: xylanase (1,4-β-D-xylan xylanohydrolase; EC 3.2.1.8), which hydrolyzes the β-1,4-xylosidic linkages of the xylan backbone; and, the β-xylosidase (1,4-β-D-xylan xylohydrolase; EC 3.2.1.37), which catalyzes the hydrolysis of 1,4-β-D-xylans, removing D-xylose from the non-reducing termini. Based on their primary sequence, β-xylosidases have been grouped into five types: the so-called glycoside hydrolase families, GH, 3, 39, 43, 52 and 54, available on the carbohydrate-active enzymes server (the CAZy database: http://afmb.cnrs-mrs.fr/CAZY/). To date, there are only three-dimensional structures of members belonging to GH39 and GH43 families. Xylosidases have received wide attention since they can be used for oligosaccharide synthesis [11];

Abbreviations: CD, circular dichroism; DEO, 1-deoxynojirimycin; DTNB, 5, 5′-dithiobis-2-nirobenzoic acid; GH, glycoside hydrolase; GdmCl, guanidine hydrochloride; $[GdmCl]_{1/2}$, the chemical-denaturation midpoint; ITC, isothermal titration calorimetry; p-NPX, p-nitrophenyl-β-D-xylanopyranoside; R_s, Stokes radius; β-xylosidase^{gp}, β-xylosidase from *Geobacillus pallidus*; XynB2, intracellular β-xylosidase from *Geobacillus stearothermophilus*; UV, ultraviolet

* Corresponding authors. L.M. Contreras is to be contacted at tel.: +58 2418688462; fax: +58 2418688462. J.L. Neira, Instituto de Biología Molecular y Celular, Edificio Torregaitán, Universidad Miguel Hernández, Avda. del Ferrocarril, s/n, 03202, Elche (Alicante), Spain. Tel.: +34 966658459; fax: +34 966658758.
E-mail addresses: contrera@uc.edu.ve (L.M. Contreras), jlneira@umh.es (J.L. Neira).
[1] On sabbatical leave in Universidad Miguel Hernández, Elche (Alicante), Spain.

1570-9639/$ – see front matter © 2008 Elsevier B.V. All rights reserved.
doi:10.1016/j.bbapap.2008.06.019

then, it is important to obtain as much structural and biophysical information as possible of β-xylosidases for their proper use in biotechnological or synthetic applications.

Geobacillus stearothermophilus is a Gram-positive thermophilic soil bacterium with an extensive hemicellulolytic system. To degrade xylan, *Geobacillus stearothermophilus* secretes an endo-1,4-β-xylanase that digests the polymer into xylooligomers. These products are taken by specific sugar transporters, and the final degradation occurs within the cells with hemicellulases [12-14]. XynB2 is an intracellular multidomain β-xylosidase belonging to the GH52 family with glyconsynthase activity [11]. Its kinetic and enzymatic properties against several substrates have been described [15], but no clue about its structural and biophysical properties have been reported. In this work, we describe the functional, structural and conformational properties of XynB2. We show that the protein was dimeric, as concluded from analytical ultracentrifugation and gel filtration chromatography; furthermore, the active site was shared between both protomers and involved aromatic residues. The protein was mainly composed by α-helix (30%) and β-sheet (30%) secondary structures, as shown by CD and FTIR. We also carried out the kinetic characterization of XynB2 with respect to its thermal stability. Our results revealed that XynB2 was kinetically thermostable, with an optimum activity temperature of 70 °C. We have recently reported the first structural features of a GH52 β-xylosidase protein [16], which allows us to compare the structural features of both proteins and to obtain general clues on the conformational properties of this family of enzymes. The comparison indicates that percentages of secondary structure and the biophysical properties are generally conserved among the members of the same family.

2. Materials and methods

2.1. Materials

Restriction enzymes, T4 DNA ligase, and the thermostable *Pwo* polymerase were purchased from Roche Diagnostic S.L. (Spain). The β-mercaptoethanol was from BioRad (USA), and the Ni^{2+}-resin was from GE Healthcare (USA). The molecular mass marker was from GE Healthcare. Urea and GdmCl ultra-pure were from ICN Biochemicals (USA). Exact concentrations of urea and GdmCl were calculated from the refractive index of the solutions [17]. Dialysis tubing with a molecular weight cut-off of 3500 Da was from Spectrapore (UK). Water was deionized and purified on a Millipore system.

2.2. Cloning of the XynB2 gene

Geobacillus stearothermophilus CECT 43, 49 and NCIB8224 were used as possible donors of the β-xylosidase gene. These strains were grown at 30 °C for 20 h in LB, to extract chromosomic DNA. DNA of three *G. stearothermophilus* strains for PCR amplification of β-xylosidase gene was extracted as described [18]. The primers used were designed based on the GenBank sequence D28121 [19]: XynB2-5 (5′-CGAAGCTTATGACAGGAAATATTCATGCCAACCAATCTATTTTT-3′), and XynB2-3 (5′-GGTACCTTAATGATGATGATGATGTTCTCCCTCCT-CAAGCC-3'). The latter included a polyhistidine tag (His_6-tag) before the stop codon. The HindIII and KpnI digested 2118 bp fragment was purified from agarose gel using QIAquick (Qiagen) and ligated into pBluescript II SK (+) plasmid (pBSK, Stratagene Cloning Systems) to create plasmid pJAVI91.

2.3. Protein expression and purification

Escherichia coli C43 cells [20] were transformed with the pJAVI91 plasmid. Recombinant XynB2 was purified by using Ni^{2+}-chromatography in buffer Tris (50 mM, pH 8), with a 0 to 1 M gradient of imidazol, and finally, by using gel filtration chromatography with a Superdex 200 16/60 gel filtration column (GE Healthcare) in 50 mM Tris buffer (pH 7.0) and 150 mM NaCl running on an AKTA-FPLC system (GE Healthcare). The final XynB2 yield was 30–35 mg of protein per liter of culture. The samples were dialysed extensively against water, lyophilized and stored at −80 °C. Protein concentration was calculated from the absorbance at 280 nm, using the extinction coefficients of model compounds [21]. Samples for chemical-denaturation studies were prepared by dissolving the lyophilized protein either in deionized water (unfolding) or in 7 M GdmCl (refolding).

2.4. Assay of β-xylosidase activity

The XynB2 activity assay was based on the colour reaction of p-nitrophenyl-β-D-xylanopyranoside as described [16,22]. One unit of β-xylosidase activity was defined as the release of 1 μmol of p-nitrophenol in 1 min. The absorbance was measured in a Shimadzu UV-1603 spectrophotometer (Japan).

2.5. Changes in the activity of XynB2 upon temperature and kinetics of thermal inactivation

The effect of temperature on the enzymatic activity was determined by performing the assay at different temperatures, in 25 mM phosphate buffer (pH 6.5). The temperature dependence of the activity was analyzed by using an Arrhenius plot ($\ln(V_{max})$ *versus* $1/T$), and the activation energy, E_a, was determined from its slope.

The protein thermostabiliy was measured as a loss of activity by incubation of the protein for 15 min at selected temperatures; the residual activity was measured at 70 °C, which is the temperature of maximum activity (see below), after cooling to 4 °C.

The kinetics of thermal inactivation of XynB2 was studied at 65, 70 and 75 °C. The time-course of enzyme inactivation was followed by taking samples at selected times; those samples were then cooled and assayed. The residual activity was measured and expressed as a percentage of the initial activity. The data were fitted to a first-order reaction, and the inactivation rate constants, k, at the three temperatures were used to calculate the E_a, according to the Arrhenius equation [23]. The activation enthalpies of XynB2 at each temperature were calculated from: $\Delta H^{\#} = E_a - RT$ [23]; the values for the activation free energy, $\Delta G^{\#}$, and the activation entropies , $\Delta S^{\#}$, were calculated as described [23].

2.6. Kinetic analysis of the enzymatic reaction

The K_m and k_{cat} constants for the p-NPX reaction were determined by varying the concentration of substrate between 0 and 2 mM in the presence of 8 nM of XynB2 at 50 °C, in phosphate buffer (25 mM, pH 6.5). Data were generated continuously as the reaction proceeded. Fitting by non-linear least-squares analysis to the Michaelis–Menten equation [24] was carried out by using the general curve fit option of Kaleidagraph (Abelbeck software) working on a PC computer.

2.7. Gel filtration chromatography

The standards used in column calibration, and their corresponding Stokes radii were those described previously [16,25,26]. Gel filtration chromatography was used to determine the Stokes radius, R_s, of the predominant species [16,27,28]. In the experiments at different pHs, the buffers (see below) were used at a final concentration of 50 mM with 150 mM of NaCl to avoid interactions with the column.

2.8. Determination of the free thiol groups

The concentration of the free thiols in XynB2 was determined by measuring the absorbance at 412 nm, following the reaction of DTNB [29]. Samples were incubated at 25 °C for 1 h. Experiments were

carried out in sodium phosphate pH 6.5, either in aqueous solution or in the presence of 6 M GdmCl.

2.9. Isothermal titration calorimetry (ITC)

ITC experiments were carried out by using a VP-ITC instrument (MicroCal Inc., USA), at four temperatures below the denaturation thermal midpoint to avoid the unfolding reaction, and to allow the calculation of the heat capacity of the binding reaction, ΔC_p of XynB2 to DEO; we used DEO because is a potent inhibitor for XynB2 [15]. Calculation of the thermodynamic parameters of the binding reaction could provide some clues on the conformation or structure of the active site.

Prior to the experiment, XynB2 was concentrated and dialysed at 4 °C against the working buffer (phosphate, pH 6.5, 50 mM). The calorimetric cell was loaded with XynB2, and microliter amounts (3 μl) of ligand inhibitor solution (DEO) were added sequentially to the calorimetric cell (1.41 ml) until all the available binding sites were saturated. The amount of power required to maintain the reaction cell at constant temperature after each injection was monitored as a function of time. The exchanged heat due to the binding reaction between DEO and XynB2 was obtained as the difference between the heat of reaction and the corresponding heat of dilution (by injecting the inhibitor to the calorimetric cell containing buffer). The resulting isotherm (individual apparent enthalpy changes upon binding *versus* molar ratio, [XynB2]/[DEO]) was fitted to a single-site model assuming that all the binding sites in the protein were identical. The thermodynamical parameters of binding were obtained by analyzing the data with the software package Origin 7.0 provided by MicroCal.

2.10. Analytical utracentrifugation

Sedimentation equilibrium experiments were performed at 25 °C in an Optima XL-A (Beckman-Coulter Inc.) analytical ultracentrifuge equipped with UV-visible optics, using an An50Ti rotor, with a 3 mm double-sector charcoal-filled Epon centerpiece. Samples of freshly dialyzed XynB2 at 15 μM in 50 mM Tris–HCl (pH 7.5) were loaded into the cell, and the dialysate was transferred to the reference sector. The velocities used were 3000 (10,920 g), 5000 (18,200 g), 6000 (21,840 g), 7000 (25,480 g), 9000 (32,760 g) and 42,000 (152,880 g) rpm. Short column (23 μl) low speed sedimentation equilibrium was performed at 6000 rpm, and the system was assumed to be at equilibrium when the successive scans overlaid. The equilibrium scans were obtained at 280 nm. The baseline signal was measured after high speed centrifugation (5 h at 42,000 rpm). The whole-cell apparent molecular weight of the protein was obtained with the program EQASSOC [30], and the goodness of the fitting was judged by the values of residuals (in all cases within less than ±0.02).

The sedimentation velocity experiment was carried out in an XL-A analytical ultracentrifuge (Beckman-Coulter Inc.) at 42000 rpm and 25 °C, using an An50Ti rotor and 3 mm charcoal-filled Epon double-sector centerpiece. Absorbance was measured at 280 nm. Protein concentration was 20 μM in 50 mM Tris (pH 7.5). Data were modelled as a superposition of Lamm equation solutions with the SEDFIT software (available at www.anlyticalultracentrifugation.com/default.htm) [31]. The sedimentation coefficient distribution, $c(s)$, was calculated at a confidence level of $p=0.68$. The experimental sedimentation values were determined by integration of the main peak of $c(s)$ and corrected to standard conditions to get the corresponding $s_{20,w}$ values with the SEDNTERP program [32]. Calculation of frictional coefficient ratio was performed with the SEDFIT program to obtain the $c(M)$ distribution [31].

2.11. Fluorescence

All fluorescence spectra were collected on a Cary Varian (USA) spectrofluorimeter, interfaced with a Peltier unit, at 25 °C. The concentration of XynB2 was 2 μM (in protomer units), and the final concentrations of the used buffers (see below) were, in all cases, 10 mM. A 1-cm-pathlength quartz cell (Hellma) was used.

2.11.1. Steady-state fluorescence measurements

Protein samples were excited at 280 and 295 nm [33]. The slit widths were equal to 5 nm for the excitation and emission light. The fluorescence experiments were recorded between 300 and 400 nm. The signal was acquired for 1 s and the increment of wavelength was set to 1 nm. Blank corrections were made in all spectra.

The chemical-denaturations, either followed by fluorescence or CD (see below), were carried out at pH 6.5 or 7.0. Samples were incubated overnight at 4 °C, and 1 h more at 25 °C.

In the pH-induced unfolding experiments, the pH was measured after completion of the experiments. The pH was measured with a thin Aldrich electrode in a Radiometer (Copenhagen) pH-meter. The salts and acids used were: pH 2.0–3.0, phosphoric acid; pH 3.0–4.0, formic acid; pH 4.0–5.5, acetic acid; pH 6.0–7.0, NaH_2PO_4; pH 7.5–9.0, Tris acid; pH 9.5–11.0, Na_2CO_3; pH 11.5–12.0, Na_3PO_4.

2.11.2. ANS-binding

Excitation wavelength was 380 nm, and emission was measured from 400 to 600 nm. Slit widths were 5 nm for excitation and emission light. Stock solutions of ANS were prepared in water and diluted to yield a final concentration of 100 μM. In all cases, blank solutions were subtracted from the corresponding spectra.

2.11.3. Thermal experiments

Fluorescence thermal denaturations were followed by the change in the emission at 315, 340 and 350 nm after excitation at either 280 or 295 nm. Instrumental parameters and protein concentration were the same as in the steady-state measurements. Heating led to precipitation in all cases.

2.12. Circular dichroism

Circular dichroism spectra were collected on a Jasco J810 spectropolarimeter (Japan) fitted with a thermostated cell holder and interfaced with a Peltier unit. The instrument was periodically calibrated with (+) 10-camphorsulphonic acid.

2.12.1. Steady-state spectra

Isothermal wavelength spectra at different pHs were acquired at a scan speed of 50 nm/min with a response time of 2 s and averaged over four scans at 25 °C. Far-UV measurements were carried out at 2 μM of protein (in protomer units) and 10 mM of the corresponding buffer (see above), in a 0.1-cm-pathlength cell. Every pH-denaturation experiment was repeated three times with new samples. Near-UV measurements were carried out with a protein concentration of 15 μM (in protomer units), in a 0.5-cm-pathlength cell.

In the chemical-denaturation experiments, far-UV CD spectra were acquired at 25 °C with a scan speed of 50 nm/min; four scans were recorded and averaged, with a response time of 4 s. The cell pathlength was 0.1 cm, with a protein concentration of 2 μM (in protomer units). Spectra were corrected by subtracting the proper baseline in all cases. Every chemical-denaturation experiment was repeated at least three times with new samples.

The observed raw optical activity was expressed as mean residue molar ellipticity $[\theta]$ (degree cm^2 $dmol^{-1}$) [28] and the secondary structure of XynB2 was predicted by using the *CDNN deconvolution* software (available at http://bioinformatik.biochemtech.uni-halle.de/cdnn/) [34].

2.12.2. Thermal denaturations

Thermal denaturations were performed at heating rates of 60 °C/h and a response time of 8 s. Thermal scans were collected in the far-UV

region at 222 nm in 0.1-cm-pathlength cells with a total protein concentration of 2 μM (in protomer units). The conditions were the same as those reported in the steady-state experiments. Heating led to precipitation in all cases. The possibility of drifting of the CD spectropolarimeter was tested by running two samples containing buffer, before and after the thermal experiments. No difference was observed between the scans.

2.13. Analysis of the pH-and chemical-denaturation curves, and free energy determination

The average emission intensity in fluorescence spectra,<λ>, was calculated as described [35].

The pH-denaturation experiments were analysed assuming that both species, protonated and deprotonated, contributed to the fluorescence spectrum:

$$X = \frac{\left(X_a + X_b 10^{n(\mathrm{pH}-\mathrm{p}K_a)}\right)}{\left(1 + 10^{n(\mathrm{pH}-\mathrm{p}K_a)}\right)}, \quad (1)$$

where X is the physical property being observed (ellipticity, fluorescence intensity or <λ>), X_a is that of the acidic species, X_b is that at high pHs, pK_a is the apparent pK of the titrating group, and n is the Hill coefficient (which was close to 1 in all the curves reported in this work). The apparent pK_a was obtained from three different measurements, prepared with new samples. Fitting by non-linear least-squares analysis to Eq. (1) was carried out by using the general curve fit option of Kaleidagraph (Abelbeck software) working on a PC computer.

To facilitate comparison among the biophysical techniques, data were converted to the fraction of native molecules [36].

The GdmCl-chemical-denaturation curves were analysed using a two- (pH 7.0) or three-state (pH 6.5) unfolding mechanism [36], according to the linear extrapolation model used in other oligomeric proteins [37]. We first used urea as the chemical-denaturant agent, but no sigmoidal behaviour was observed during the fluorescence titrations (data not shown).

2.14. Fourier transform infrared spectroscopy

The protein was lyophilised and dissolved in deuterated buffer Tris 10 mM, and 0.1 M NaCl (pD 6.5); no pH-corrections were done for the isotope effects. Samples of XynB2, at a final concentration of 125 μM, were placed between a pair of CaF_2 windows separated by a 50 μm thick spacer, in a Harrick demountable cell. Spectra were acquired on a Bruker FTIR instrument equipped with a deuterated triglycine sulphate detector and thermostated with a Braun water bath at 25 °C. The cell container was filled with dry air.

2.14.1. Steady-state measurements

Five-hundred scans per sample were taken, averaged, apodized with a Happ-Genzel function, and Fourier transformed to give a final resolution of 2 cm^{-1}. The signal to noise ratio of the spectra was better than 1000:1. Buffer contributions were subtracted, and the resulting spectra were used for analysis. The amount of the different secondary structure components was determined as described [16]. The error in the percentage of secondary structure was estimated to be 5% [38].

2.14.2. Thermal-denaturation measurements

Thermal denaturations were carried out with a scanning rate of 50 °C/h and acquired every 3 °C. Fifty scans per temperature were averaged. Calculation of the apparent thermal midpoint, T_m, was obtained by assuming that the thermal denaturation of oligomeric XynB2 followed a two-state unfolding mechanism [37].

3. Results

3.1. Thermal and kinetic features of the XynB2 enzymatic reaction

Recombinant XynB2 was purified to homogeneity by using Ni^{2+}-affinity and gel filtration chromatographies. We carried out an extensive thermal and kinetic characterization of the hydrolysis of p-NPX, to allow comparison with previous measurements in a different recombinant species of the protein, where the cell extract is heated during purification [22]. The DTNB assay shows that out of thirteen cysteines in each protomer, three are free and solvent-exposed, as concluded from the assay in the presence of GdmCl.

XynB2 showed maximal activity at 70 °C, which was 5 °C higher than the previously reported temperature [22] (data not shown). This difference is due to the purification protocol, since previous work involved a heating step during protein isolation; with the His-tagged protein this step is not longer necessary. The right-hand site of the Arrhenius plots were linear yielding a E_a of 11.0±0.3 kcal mol^{-1}, within the range obtained for other enzymatic reactions (7.6–11.5 kcal mol^{-1}) [39,40]. The K_m and k_{cat} values measured at pH 6.5 and 50 °C were 0.152±0.06 mM and 107±4 s^{-1}, respectively.

The thermostability behaviour of XynB2 shows a sharp transition, with a midpoint in the activity at 77 °C (data not shown); furthermore, the protein retained a 75, 50 and 30% of the activity after 15 min at 75, 78 and 80 °C, respectively. These findings indicate that the thermostability of XynB2 is high, but it is lower than that of other thermostable β-xylosidases [41].

Besides the question at which temperature an enzyme shows the maximal activity, it is important to consider its enzymatic use for biotechnological applications, that is, how long a specific level of activity lasts at a particular temperature. To that end, the resistance of XynB2 to irreversible heat inactivation was monitored by exposing the enzyme to long incubation times at 65, 70 and 75 °C, and then measuring the residual activity. Heat inactivation of XynB2 activity was analyzed according to the Lumry–Eyring kinetic model [42]. Heat inactivation followed a first-order kinetics (data not shown), at the three temperatures. The inactivation constants showed an Arrhenius behaviour with an E_a of 82±9 kcal mol^{-1}, in agreement with values reported in enzymes of similar molecular weight [43]. The activation parameters ($\Delta S^{\#}$, $\Delta H^{\#}$ and $\Delta G^{\#}$) for the inactivation reaction are positive as expected [43–45]; moreover, the values of $\Delta G^{\#}$ are similar to those of the xylanase from *Bacillus stearothermophilus* [44]. The half-life time ($t_{1/2}$) and inactivation constants (k_d) further indicate that XynB2 showed a high kinetic stability (Table 1).

3.2. XynB2 is a dimeric protein

We used three different biophysical probes to address the oligomerization of XynB2. One of them, in addition, provided us with the thermodynamic parameters of the binding reaction of DEO.

Table 1
Activation parameters of the irreversible enzymatic thermal denaturation of XynB2[a]

t (°C)	$T_{1/2}$[b] (h)	$k_d \times 10^{-4}$[b] (s^{-1})	$\Delta H^{\#}$ (kcal mol^{-1})	$\Delta G^{\#}$ (kcal mol^{-1})	$\Delta S^{\#}$ (cal mol^{-1} K^{-1})
65	19.20	0.10	81.06	27.60	158.17
70	3.40	0.56	81.05	26.84	158.07
75	0.46	4.19	81.04	25.81	158.57

[a] E_a=82±9 kcal mol^{-1} (calculated from the Arrhenius plot of ln (k_d)).
[b] Half-life times ($t_{1/2}$) and thermal inactivation constants (k_d) were calculated from plots of residual activity ($\ln(A/A_0)$, where A is the absorbance at any time, and A_0 is the absorbance at the beginning of the reaction) *versus* time.

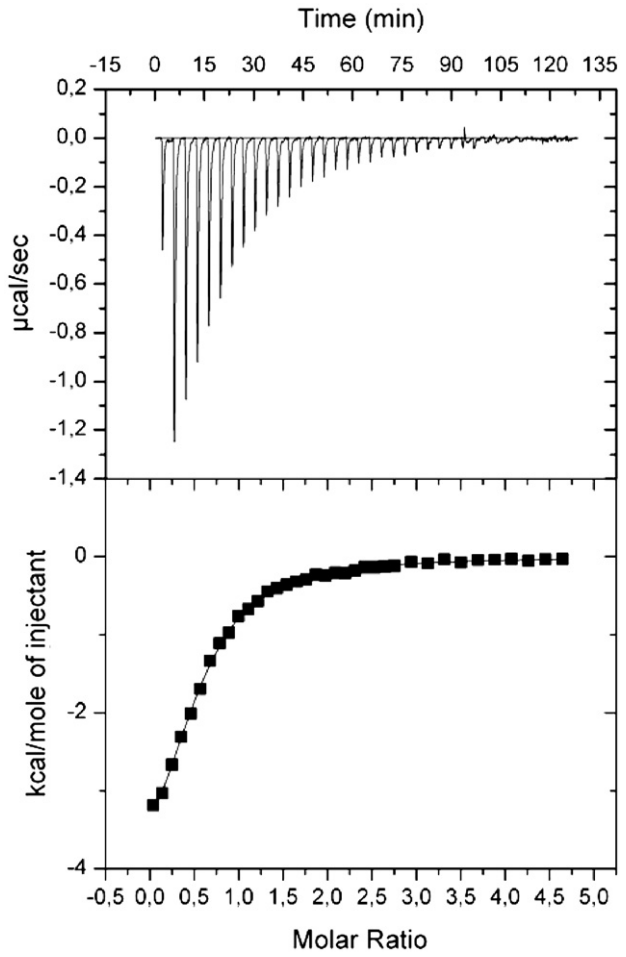

Fig. 1. ITC measurements. The top trace shows the raw data at 15 °C. XynB2 at 100 µM in the calorimetric cell was titrated with DEO (at 5 mM concentration). Successive amounts of DEO were added to the cell (3 µl) until all the binding sites were saturated. The lower trace is the fitting of data after signal integration. Experiments were acquired at pH 6.5 (sodium phosphate buffer, 50 mM).

3.2.1. ITC binding studies

The calorimetric titrations (Fig. 1) are consistent with a stoichiometry of one molecule of inhibitor binding to two molecules of XynB2 (Table 2) suggesting that there is a single catalytic site comprising residues of both monomers; other GH52 β-xylosidases characterized to date are also dimeric, but no clue about the location of the active site had been provided so far [22,46-48]. The binding reaction has a free energy of −6.1 kcal mol^{-1} at 25 °C (consistent with a binding constant of $3 \cdot 10^4$ M^{-1}). The binding process is enthalpically driven (ΔH amounts −5.72 kcal mol^{-1} at room temperature), while the entropic contribution to the free energy of binding ($-T\Delta S$ is −0.4 kcal mol^{-1} at this temperature) becomes more unfavourable as the temperature is raised. Finally, the heat capacity change is fairly small and negative (−97 cal K^{-1} mol^{-1}) suggesting that: (i) the binding of the inhibitor to the protein does not induce major conformational changes; and, (ii) the inhibitor has stacking interactions with an aromatic residue [49].

Table 2
Binding parameters of the association-dissociation reaction of XynB2 with DEO[a]

t (°C)	n[b]	$K_b \times 10^{-4}$ (M^{-1})	K_d (µM)	ΔG (kcal mol^{-1})	ΔH (kcal mol^{-1})	ΔS (cal K^{-1} mol^{-1})
5	0.533	4.6	21.8	−5.9	−3.6	8.2
15	0.531	3.9	25.8	−6.0	−4.8	4.2
25	0.557	3.0	33.4	−6.1	−5.7	1.3
35	0.539	2.4	40.8	−6.2	−6.6	−1.3

[a] The protein solution (in the calorimetric cell) varied from 100 to 112 µM (depending of the stock solution), while the concentration of the inhibitor (used as titrating agent) ranged from 5 to 7.5 mM.

[b] The n value is the apparent stoichiometry of the protein/inhibitor complex (number of protein monomers per molecule of inhibitor in the complex), with the average of the four experiments being 0.54±0.01. K_b refers to the binding constant and K_d stands for the dissociation constant ($K_d = 1/K_b$). The thermodynamical state functions for the binding process, ΔG, ΔH and ΔS, are reported.

3.2.2. Gel filtration

The protein eluted at pH 7.0 at 11.47 ml in a Superdex 200 HR 16/60 column, which yields a hydrodynamic radius of 44.2 Å [16,27,28] (Fig. 2). We can compare this value with that expected for an anhydrous dimeric sphere, with a $\overline{V} = 0.703$ cm^{-3} g^{-1} [50], which is 36.5 Å. The discrepancy could be due to: (i) a deviation of the molecular shape from a sphere, since an elongated XynB2 should elute at a smaller volume in the gel filtration experiments; or, alternatively, (ii) a highly hydrated molecule. We can further elaborate on the latter hydration issue, by considering that all deviations from the radius of an ideal sphere are due to the hydration effects [27]:

$$w_{max} = \frac{\overline{V}}{\overline{V}_{water}} \left[\left(\frac{R_s}{R_0} \right)^3 - 1 \right],$$

where $\overline{V}_{water}$ is the partial specific volume of water (1 cm^3 g^{-1}), $\overline{V}$ is the specific volume of the protein (see above), R_s is the experimentally determined Stokes radius, R_0 is that determined for an ideal anhydrous sphere, and w_{max} is an upper limit for the protein hydration (in grams of bound water per gram of protein). The w_{max} for globular proteins is usually 0.3 g of water per gram of protein, or even lower [27]; the w_{max} of XynB2 was 0.65 g of water per gram of protein, suggesting that, if that is spherical, it is highly hydrated.

3.2.3. Analytical ultracentrifugation

The confirmation of the dimeric nature of the protein was obtained from sedimentation equilibrium measurements at pH 7.5, since the distribution of mass along the cell could be fitted to a solute with an apparent molecular mass of 156.2 kDa, very close to the calculated 159.7 kDa for a dimeric β-xylosidase (Fig. 3A).

In the sedimentation velocity experiments at pH 7.5 a single species was observed with an estimated molecular weight of 153.7 kDa (Fig. 3B), slightly smaller than that obtained by sedimentation equilibrium and from theoretical estimations. This underestimation of the experimental molecular weight suggests that the shape of the molecule deviates from that of a sphere, which is consistent with the results from gel filtration chromatography (see above).

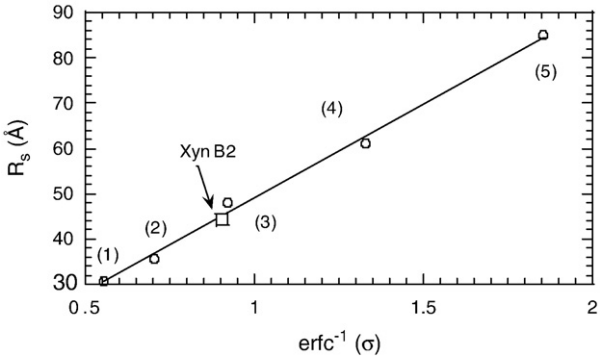

Fig. 2. Hydrodynamic properties of XynB2. Determination of the R_s of XynB2 at pH 7.0. The elution volume of the protein is indicated by an arrow. The numbering corresponds to the elution volumes of ovalbumin (1), albumin (2), aldolase (3), ferritin (4) and thyroglobulin (5). The equation was: $R_s = 41.6 \times \text{erfc}^{-1}(\sigma) + 7.39$ (with a regression coefficient of 0.99).

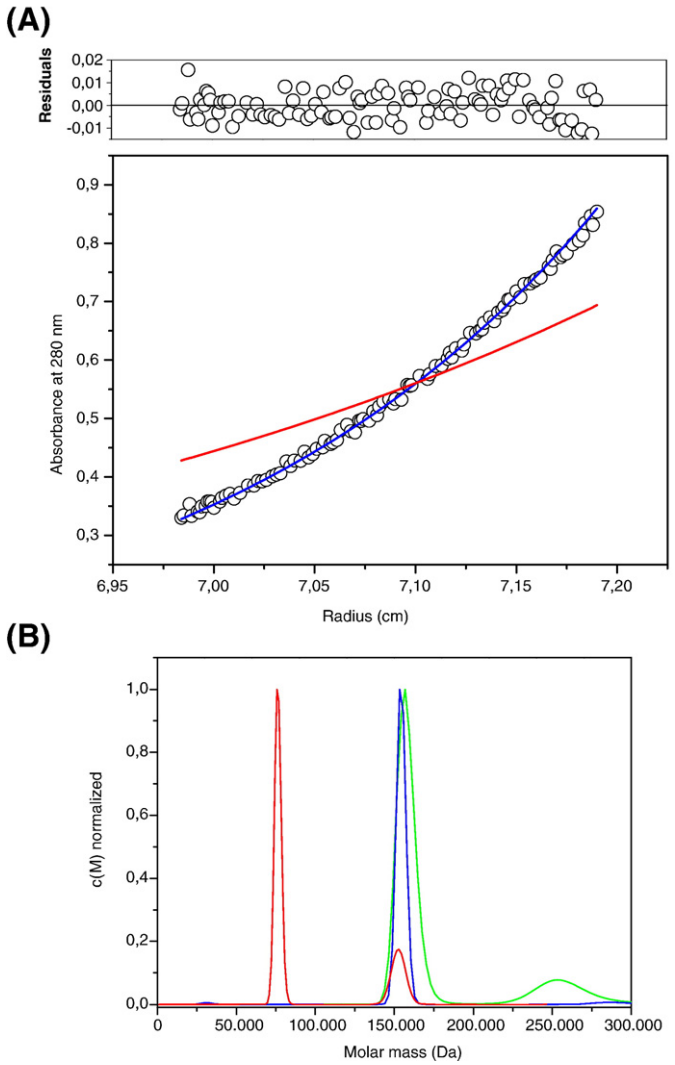

Fig. 3. Analytical ultracentrifugation analysis of XynB2. (A) Representative sedimentation equilibrium experiment (blank circles) at pH 7.5; the fitting and residuals for a dimeric species (blue line) are shown. The fitting (red line) to a monomer species is also indicated. Sedimentation equilibrium was determined at several speeds (representative data for 6000 rpm are shown), at 25 °C and at 15 μM of protein. (B) Concentration distribution *versus* molecular weight of the different oligomeric states of XynB2 at pH 4 (red line), pH 7.5 (blue line) and pH 9.0 (green line).

The sedimentation velocity analysis at pH 9.0 indicate that the protein is a dimer (with a molecular weight of 153.7 kDa), but at pH 4.0, XynB2 is predominantly a monomer (with a molecular weight of 76 kDa) (Fig. 3B).

3.3. The structure and pH-induced conformational changes of XynB2

3.3.1. Structure of XynB2 at pH 7.0

The secondary structure of XynB2 was examined at 25 °C by FTIR and CD using deconvolution procedures. The far-UV CD spectrum of the protein showed a broad minimum between 220 and 210 nm (Fig. 4A), which suggests the presence of α-helix-or turn-like conformations together with β-sheet [51,52]. Deconvolution of the CD spectra by using the CDNN program [34] yields a 30.3% of helical structure, a 20.3% of β-sheet, a 17.5% of β-turns, and a 32.2% of random-coil structure, similar to the values obtained by deconvolution of the FTIR spectra (Table 3).

Near-UV spectra gives information on the asymmetric environment of the aromatic residues [51,52]. The near-UV of XynB2 is very rich, with a broad minimum at 268 nm, two others at 280 and 288 nm,

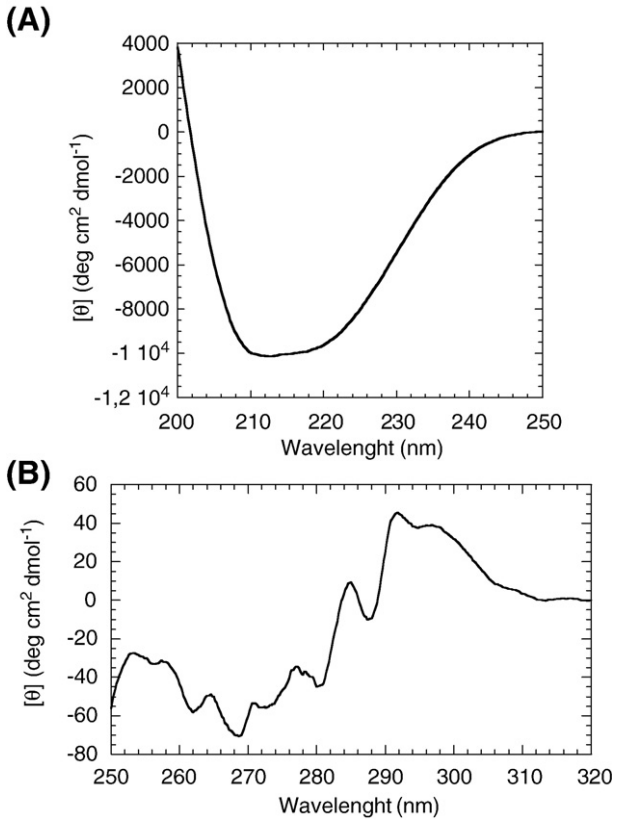

Fig. 4. Circular dichroism of XynB2. (A) Far-UV spectrum acquired in 0.1-cm-pathlength cells. (B) Near-UV spectrum acquired in 0.5-cm-pathlength cells. Conditions were pH 6.5 (sodium phosphate buffer) and 25 °C and a concentration of 2 μM for the far-UV experiments and 20 μM for the near-UV spectrum.

and a small maximum at 295 nm (Fig. 4B). The tryptophan contribution to the XynB2 spectrum suggests a very intense L_b transition; and the minima indicate prominent vibrational bands at 270 and 290 nm, probably due to solvent-exposed aromatic residues [53,54].

3.3.2. The pH-conformational changes

To characterize the structure and the stability of XynB2 we used intrinsic and ANS steady-state fluorescence and CD.

3.3.2.1. Steady-state fluorescence spectroscopy. We used fluorescence to monitor changes in the tertiary structure of the protein, around the seventeen tryptophans and the twenty-nine tyrosines *per* monomer [33]. The emission fluorescence spectrum of XynB2 at a concentration of 2 μM (in protomer units) had a maximum at 342 nm at neutral pHs, and then, it was dominated by the emission of the tryptophan residues. From the blue-shifted maxima, we can conclude that the tryptophans (or at least one of them, dominating the spectrum) are completely buried in the structure. The changes in the intensity at 340 nm (either by excitation at 280 or 295 nm) showed two titrations (Fig. 5A, filled squares). The pK_a of the titration at low pH was 4.2 ± 0.1 (at both excitation wavelengths), similar to that observed for solvent-

Table 3
Secondary structural analysis of XynB2 at pH 6.5 as determined by FTIR[a]

Wavenumber (cm^{-1})	Structural assignment	% of total secondary structure
1670–1685	β-turns	17
1657	α-helix	31
1646	Random-coil	22
1627–1640	Anti-parallel β-sheet	30

[a] Errors in the wavenumber are estimated to be ±2 cm^{-1}.

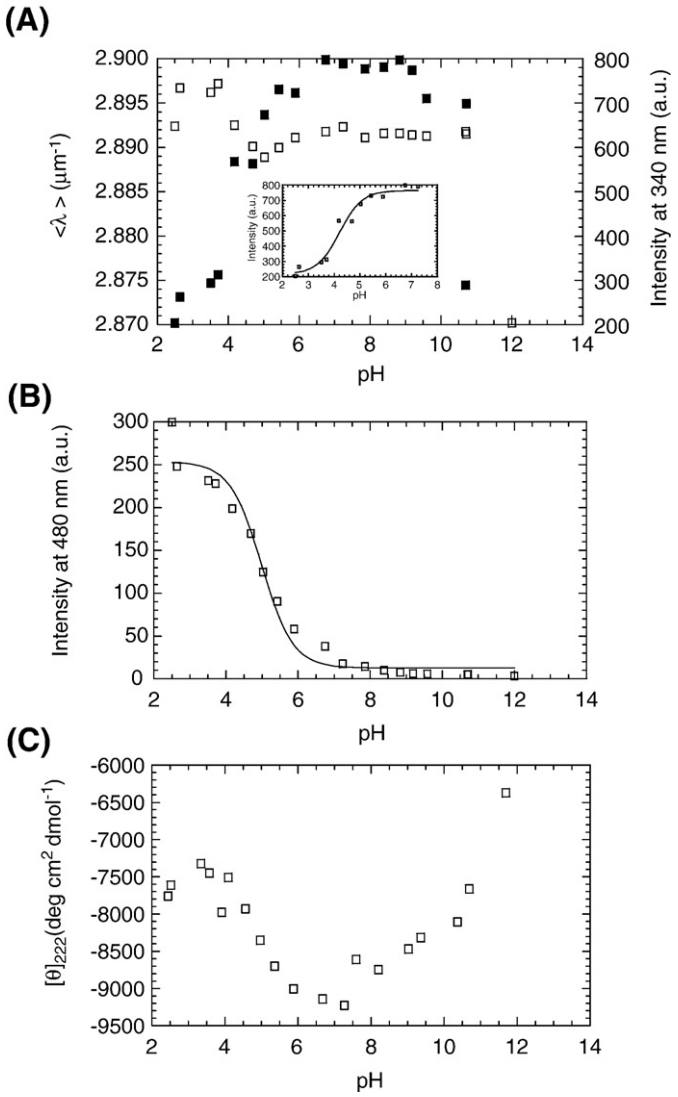

Fig. 5. pH-induced structural changes of XynB2 followed by fluorescence and CD. (A) Intrinsic fluorescence: The <λ> (blank squares) and the intensity at 340 nm (filled squares) obtained by excitation at 280 nm are represented *versus* the pH. The inset is the fitting of the intensity at 340 nm in the acidic region to Eq. (1). (B) Fluorescence intensity of ANS at 480 nm. The ANS concentration was 100 μM. The line through the data is the fitting to Eq. (1). (C) The ellipticity at 222 nm *versus* pH. The spectra were acquired in 0.1-cm-pathlength cells. For all spectroscopic experiments, protein concentration was 2 μM (in protomer units) and buffer concentration was 10 mM.

exposed glutamic residues (4.25±0.05) [55]. Conversely, we could not determine the pK_a of the titration at basic pH, which is probably related with the deprotonation of some, if not all, of the tyrosine, arginine or lysine residues [55]. The profile of <λ> showed also two titrations; the one at low pH had an apparent pK_a of 4.0±0.3, similar to that obtained by following the intensity at 340 nm (Fig. 5A, blank squares).

3.3.2.2. ANS-binding. ANS-binding was used to monitor solvent-exposed hydrophobic regions [56]. At low pH, the fluorescence intensity at 480 nm was large and decreased as the pH was raised (Fig. 5B), suggesting that the protein is exposing hydrophobic regions. The intensity at 480 nm showed a sigmoidal behaviour with a pK_a=4.43±0.08, similar, within the error, to that determined by intrinsic fluorescence (Fig. 5A).

3.3.2.3. Far-UV CD. We used far-UV CD as a spectroscopic probe that is sensitive to protein secondary structure [51,52]. The experiments were carried out at the same concentration as in fluorescence experiments (2 μM, in protomer units). The shape of the CD spectrum did not change between pH 6 and 8.5. The behaviour of the ellipticity at 222 nm was, however, different to that observed by <λ> and the intensity at 340 nm (see above): the ellipticity decreased steeply (in absolute value) at very acidic or basic pH values (Fig. 5C). We could not determine the midpoint of the transition at acidic pH due to the data scattering of the acidic baseline. Then, we can conclude that the acquisition of secondary (as monitored by far-UV CD) did not occur at the same pHs as the acquisition of tertiary structure (fluorescence).

3.3.2.4. Thermal denaturations at different pHs. Thermal denaturations were irreversible above pH 6, with apparent thermal midpoints close to 80 °C (data not shown), and then, we did not try to obtain any

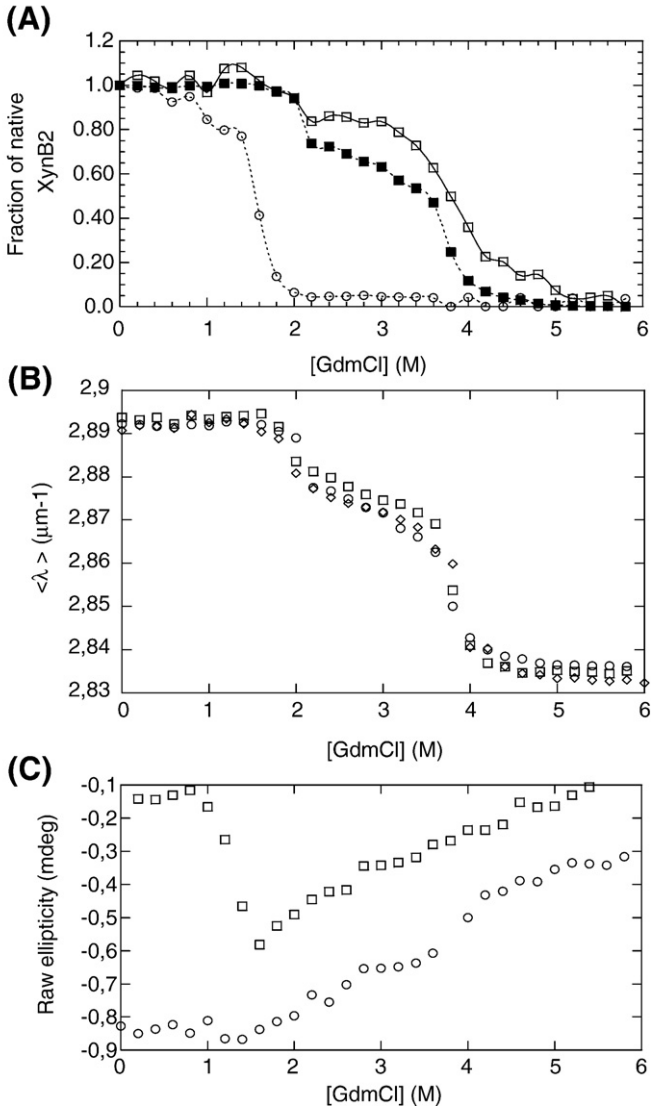

Fig. 6. Chemical-denaturation of XynB2 followed by CD, fluorescence and activity at pH 6.5. (A) Fraction of native protein followed by CD (ellipticity at 222 nm, blank squares), fluorescence (<λ>, filled squares) and activity (blank circles). The lines are drawn to guide the eye. Protein concentration was in all cases 2 μM (in protomer units) at 25 °C. The fitting of CD data for the first transition led to: $[GdmCl]_{1/2}$=1.97±0.07 M; and for the second one: $[GdmCl]_{1/2}$=3.76±0.08 M. (B) The <λ> at different concentrations of XynB2 (in protomer units): 1 μM (blank diamonds); 2 μM (blank squares) and 3 μM (blank circles) measured at 25 °C. (C) Raw data for the ellipticity at 222 nm in the unfolding (blank circles) and refolding of XynB2 (blank squares) at 25 °C (the units on the *y*-axis are arbitrary).

thermodynamic parameter; below pH 6, however, no sigmoidal behaviour was observed (data not shown). Denaturations were concentration-independent (within the 2 to 20 μM range), but they were scan-rate-dependent. The activation energy, E_a, of the kinetic irreversible denaturation process, was 135±20 kcal mol^{-1}, as determined by the method developed by Sánchez-Ruiz and co-workers [57–59].

3.4. The chemical-denaturation of XynB2

Since protein stability could not be determined by thermal denaturation, we tried to calculate it by means of chemical-denaturation. We observed a sigmoidal transition, when denaturation was followed by CD, fluorescence or activity at pH 6.5 (Fig. 6A). The spectroscopic techniques showed two transitions and the activity measurements a single one, which occurred at slightly smaller [GdmCl] (~1.8 M) than the first one observed by the biophysical techniques (~2.0 M). We carried out fluorescence measurements at different XynB2 concentrations (Fig. 6B); although it was difficult to fit the data of the first transition, the results suggest, within the experimental error, a slight concentration-dependence of the first transition, and then, this transition must involve a second-order molecular event. It is important to note, however, that the protein-concentration-dependence evidence was weak, since in all cases, the variations of the $[GdmCl]_{1/2}$ are within the experimental error.

Conversely, we did not observe a concentration-dependence in the second transition observed by the spectroscopic techniques, suggesting that it involves a single-molecular event. Chemical-denaturations were also followed by the change in the ANS fluorescence (data not shown), showing two transitions: (i) the first one involved an increase of the intensity at 480 nm, with a $[GdmCl]_{1/2}$=2.1±0.4 M; and, (ii) a second one, where the intensity at 480 nm decreased, with a $[GdmCl]_{1/2}$=3.85±0.02 M. These values are similar to those obtained by following the changes in the intrinsic fluorescence (Table 4). In addition, we carried out chemical-denaturation experiments at pH 7, where a single broad transition was observed either by fluorescence or CD (Table 4), with a midpoint close to the mean of the $[GdmCl]_{1/2}$s observed at pH 6.5 (2.65±0.05 M).

We finally tested whether, the chemical-denaturations at pH 6.5 were reversible, to calculate the unfolding free energy. We did not observe a regain of protein activity at the lower GdmCl concentrations assayed (below 1.0 M GdmCl, data not shown). Further, the refolding curve, followed either by fluorescence or CD, showed a hysteresis behaviour (Fig. 6C), and, then, it was not possible to obtain any thermodynamic parameter. Hysteresis behaviour has been explained as due to kinetic phenomena, and to test this hypothesis, we measured the denaturation of XynB2 at different times since its preparation (Table 4). The first concentration-dependent transition was not time-dependent, but the second concentration-independent transition was time-dependent.

4. Discussion

4.1. The structure and the oligomerization state of XynB2 at the optimum pH: comparison with other xylosidades of the GH52 family

To date, no three-dimensional structure of a member of the GH52 xylosidase family has been reported; recently, we have described the percentages of secondary structure of a xylosidase from *G. pallidus*, β-xylosidase^{gp} by using FTIR [16]. The percentage of helical structure of β-xylosidase^{gp} is similar to that observed in XynB2, although XynB2 seems to contain a larger percentage of disordered structure (Table 3). Further, β-xylosidase^{gp} acquires a native-like structure around pH 6, and the environment around the tryptophan and tyrosine residues remains unchanged up to pH 9 [16]; this pH range is similar to that described in this work for XynB2 (see below). Then, although the percentages of secondary structure in both GH52 proteins are slightly different, the acquisition of native-like features occurs in a similar way.

We can compare the thermodynamic parameters of the binding reaction of DEO with those measured for other xylooligomers [15]. The ΔH for the binding of xylotriose at 30 °C is similar to that measured here for DEO, but the binding constant of DEO to XynB2 is three-times smaller, as it could be expected for an inhibitor; the entropic term, on the other hand, is positive for DEO and xylotriose [15]. However, Shoham and co-workers observe that for xylobiose and xylotriose, the stoichiometry value of the binding reaction (as measured by ITC) is close to 1 (in contrast with the value of 0.5 determined here, Table 2). The reasons of such discrepancy are not know, but they could rely on the long size of the xylooligomers occupying several subsites at both subunits, whereas the small DEO would reside only in the active site. Furthermore, our ITC data in the presence of DEO suggest that the active site center is shared by both protomers (assuming that the binding site of the substrate is the same as that of the inhibitor). A shared active site center among the different protomers has also been observed in thermostable enzymes [60].

4.2. Irreversible thermal denaturation of XynB2: Relationship to thermostability

Small monomeric proteins tend to unfold *via* a two-state transition where unfolding intermediates are not accumulated, and regain their native and functional states after thermal- or chemical-denaturations [61]; thus, the thermodynamic parameters describing the unfolding reaction can be obtained. Conversely, large oligomeric proteins usually show intermediate states or form aggregates, upon thermal- or chemical-denaturations [62]. Then, the characterization of the folding reaction by rigorous thermodynamic analyses is not possible, and kinetic studies must be used to determine the thermostability [43,45,63].

XynB2 is a representative member of GH52 family, whose biochemical and kinetic properties have been described [22,64];

Table 4
Kinetics of the chemical-denaturation of XynB2[a]

	pH 6.5						pH 7.0	
	Activity		Fluorescence				Fluorescence	
			First transition		Second transition			
Time (days)	$[GdmCl]_{1/2}$ (M)	m (kcal mol^{-1} M^{-1})	$[GdmCl]_{1/2}$ (M)	m (kcal mol^{-1} M^{-1})	$[GdmCl]_{1/2}$ (M)	m (kcal mol^{-1} M^{-1})	$[GdmCl]_{1/2}$ (M)	m (kcal mol^{-1} M^{-1})
1	1.61±0.08	7±1	2.10±0.03	4.9±0.8	3.70±0.02	3.5±0.2	2.65±0.05	1.8±0.2
30	1.67±0.05	6.4±0.3	2.15±0.04	4.2±0.3	3.75±0.04	3.4±0.3	1.96±0.08	1.2±0.1
45							1.8±0.1	1.2±0.1
60							1.7±0.2	1.0±0.2

[a] Fluorescence data were acquired at 2 μM of protein. The values shown are those obtained by excitation at 280 nm, but similar results were obtained by excitation at 295 nm (data not shown). Chemical-denaturations were carried out at 25 °C.

however, to date no detailed study had been carried out on the relationship between its activity and stability. Our measurements indicate that the maximal activity of XynB2 occurs at high temperatures, just 7 °C below the apparent thermal midpoint, as determined by spectroscopic techniques (data not shown). Since this thermal midpoint is associated with irreversible aggregation, we can conclude that solvent-exposure of hydrophobic regions of the protein is the main determinant for the loss of activity at high temperatures. This is supported by the fact that the $\Delta S^{\#}$ of the inactivation reaction was positive, indicating that the randomness of the activation state is increased before the irreversible inactivation.

The kinetic model proposed by Lumry–Eyring allowed us to characterize the irreversible heat inactivation of XynB2, either for the enzymatic reaction (Table 1) or for folding (see Results section). Both values are different since the processes monitored are not the same: in the enzymatic reaction, we are measuring thermal inactivation in the presence of substrate (82±9 kcal mol^{-1}), and in the folding, in its absence (135±20 kcal mol^{-1}). Surprisingly, one should expect that the activation energy should be larger in the presence of substrate [24], unless the unfolding-aggregation mechanism had changed drastically. However, it is important to keep in mind that the model of Sánchez-Ruiz and co-workers [57–59] is a limiting case of a more realistic situation; such model assumes that the irreversible step is fast and the denaturation process occurs under conditions where the amount of unfolded state, U, is very low. Then, it could be due that, under our thermal-denaturation conditions, the model could not be applied. To rule out that possibility, independent DSC measurements should be carried out to determine the value of E_a; unfortunately, all the DSC measurements with XynB2 led to precipitation with large distortions of the unfolded baseline (data not shown). Notwithstanding those caveats, the kinetic barrier towards unfolding seems to be the key feature of XynB2 thermostability, as also suggested in other enzymes [63,65,66].

However, a question can be raised, why is XynB2 so thermostable? A recent comparison of sequences of proteins from thermophiles and mesophiles has provided some clues into the determinants of protein thermostability [67]. In protein sequences from thermophiles, there are a high proportions of charged (Arg, Glu and Lys) and hydrophobic (Gly, Ile, Pro and Val) residues and a low percentage of uncharged polar amino acids (Asn, Gln and Thr). In XynB2, the proportion of charged (19%) and hydrophobic residues (24%) is larger than that of uncharged amino acids (12%), suggesting that the protein is, from the point of view of the sequence, a thermostable protein. Further, since the Asn and Gln residues deaminate at high temperatures [68], the low contents of Asn (3%) and Gln (3%) in XynB2 could increase its chemical stability at higher temperatures.

4.3. The irreversible chemical-denaturation of XynB2

From the denaturation data at pH 6.5, we conclude that the functional environment around the active site is lost at very small concentrations of GdmCl (as monitored by the activity measurements), and shortly after that, secondary (CD) and tertiary (fluorescence) changes occurred. Thus, these latter techniques are monitoring dimer dissociation and, in addition, other conformational rearrangements, occurring around the active site. We can also conclude, based on fluorescence results, that tryptophan and/or tyrosine residues are involved in, or close to, the dimerization interface (as it was also suggested by the small negative ΔC_p value of the binding reaction, see Results section). These two chemical-denaturation transitions were not observed at pH 7, suggesting that there were conformational changes in the pH range from 6.5 to 7.0, as confirmed by CD (Fig. 5C) and fluorescence (Fig. 5A).

As with thermal denaturations, chemical ones were not superimposable with those from refolding experiments (Fig. 6C), precluding any thermodynamical study. Hysteresis (that is, non-superposition of the refolding and unfolding curves) is due to the non-equivalence of the unfolding and refolding, due to the fact that the unfolding and folding processes are too slow to allow equilibrium to be established within the experimental incubation times [36]. Interestingly enough, the unfolding of the monomer (the second transition observed at pH 6.5) was time-dependent, whereas the first transition was not (Table 4), suggesting that the dimer dissociation was relatively fast and it occurred within the incubation time of the experiment. However, we do not know whether the hysteresis behaviour is due to the impossibility of the isolated monomers to acquire a proper tertiary structure, or alternatively, to the inability of the well-structured monomers to assemble and dock to yield the functional native dimer. Based on the loss of ellipticity in the monomers upon refolding (Fig. 6C, blank squares), we favour the hypothesis that the isolated monomers are not capable of acquiring their native three-dimensional structure, and then the native-like monomers are not stable enough to exist isolated in solution.

4.4. The pH-induced conformational changes of XynB2

The acquisition of native-like tertiary structure from the acidic regions occurs with a pK_a of ~4.0 which is similar to that observed in a solvent-exposed glutamic residue [55]. Interestingly enough, previous site-directed mutagenesis studies propose that Glu335 and Asp495 are the key catalytic residues of XynB2 [64]; we hypothesize that since acquisition of a native-like structure from acidic pHs parallels the acquisition of an active conformation, then, the same residues responsible for protein activity are also involved (among other Asp and/or Glu residues) in folding of the enzyme (acquisition of secondary, tertiary structure compactness). Experimental pH-dependent studies on other xylosidases are necessary to confirm this suggestion in the GH52 family, although recent theoretical studies on endo-xylanases seem to pinpoint this hypothesis [69].

One question, however, remains, what is the conformational state populated at low pH, which has a large percentage of secondary structure, as shown by CD (Fig. 5C)?. Since the protein at low pH binds ANS (Fig. 5B), and it did not show a thermal-denaturation sigmoidal behaviour at acidic pHs (data not shown), we suggest that the low-pH populated species is a molten-globule [70] . In XynB2, and conversely to what happens in other oligomeric proteins [62], this species is monomeric (Fig. 3), with at least some of the tryptophans buried (as concluded from the blue-shifted wavelength at low pH, data not shown). Since the molten-globule is monomeric and it strongly binds ANS, we suggest that the dimerization interface of XynB2 is composed of inter-subunit hydrophobic (ANS-binding) and electrostatic (dissociation at low pH) interactions, with the residues involved in the interface closely clustered; this conclusion is further supported by the results of the GdmCl-denaturation experiments in the presence of ANS (data not shown), where the first transition (dimer dissociation) involved an increase of the intensity at 480 nm.

5. Conclusions

Size exclusion chromatography, analytical centrifugation, ITC, CD, fluorescence (steady-state and ANS-binding) and FTIR were used to obtain the structure, the oligomerization state and conformational changes exhibited for dimeric XynB2 when the pH, the concentration of chemical denaturants or the temperature were changed. This report describes the first extensive conformational characterization of a family 52 β-xylosidase, showing that the acquisition of native-like features occurs to pHs close to where the maximum activity is observed. Structural comparison with the scarce structural data of other xylosidases, indicates that the percentages of secondary structure seem to be conserved among the members of the GH52 family. The analysis of the structural properties suggests that the

assembly of the dimer is essential for efficient catalytic activity. Finally, since this work is the first report of the stability-activity relationships for a member of GH52 family, we plan to carry out a comparison with homologue proteins and the isolated protein-engineering designed monomeric species of XynB2.

Acknowledgements

We thank the three anonymous reviewers for their suggestions and thoughtful insights. This work was supported by Projects CTQ2005-00360/BQU (JLN), CTQ2004-07716/BQU (JG), and BIO2007-67009 (FRV) from the Spanish Ministerio de Educación y Ciencia; and Pem 2001002268 from the Venezuelan Fondo Nacional para la Ciencia y Tecnología (LMC) and 058-06 from Consejo de Desarrollo Científico y Humanístico, Universidad de Carabobo (LMC). The work of Dr. Lellys M. Contreras in Spain was partially supported by a postdoctoral fellowship from Generalitat Valenciana (Ayudas a investigadora invitada, AINV06/102) and from the Ministerio de Educación y Ciencia (Estancia de jóvenes doctores extranjeros en España, SB2005-0011). We thank Francisco N. Barrera for critical reading and suggestions. We deeply thank May García, María del Carmen Fuster and Javier Casanova for excellent technical assistance.

References

[1] R. Sackstein, J.S. Merzaban, D.W. Cain, N.M. Dagia, J.A. Spencer, C.P. Lin, R. Wohlgemuth, *Ex vivo* glycan engineering on CD44 programs human multiprotein mesenchymal stromal cell trafficking to bone, Nat. Med. 14 (2008) 181–187.
[2] A. Varki, Biological roles of oligosaccharides: all of the theories are correct, Glycobiology 3 (1993) 97–130.
[3] R.A. Dwek, Glycobiology: toward understanding the function of sugars, Chem. Rev. 96 (1996) 683–720.
[4] H.J. Gabius, Concepts of tumour lectinology, Cancer Invest. 15 (1997) 454–464.
[5] P.H. Seeberger, D.B. Werz, Synthesis and medical applications of oligosaccharides, Nature 446 (2007) 1046–1051.
[6] A. Surnakki, M. Tenkanen, J. Bucherts, L. Viikari, Hemicellulases in the bleaching of chemical pulps, Adv. Biochem. Eng. Biotechnol. 57 (1997) 261–287.
[7] J.R. Mielenz, Ethanol production from biomass: technology and commercialization status, Curr. Opin. Microbiol. 4 (2001) 324–329.
[8] L.F. Mackenzie, Q. Wang, R.A. Warren, S.G. Withers, Glycosynthases: mutant glycosidases for oligosaccharide synthesis, J. Am. Chem. Soc. 120 (1998) 5583–5584.
[9] S. Subramaniyan, P. Prema, Biotechnology of microbial xylanases: enzymology, molecular biology, and application, Crit. Rev. Biotechnol. 22 (2002) 33–64.
[10] Q.K. Beg, M. Kapoor, L. Mahajan, G.S. Hoondal, Microbial xylanases and their industrial applications, Appl. Microbiol. Biotechnol. 56 (2001) 326–338.
[11] A. Ben-David, T. Bravman, Y.S. Balazs, M. Czjzek, D. Schomburg, G. Shoham, Y. Shoham, Glyconsynthases activity of *Geobacillus stearothermophilus* GH52 β-xylosidase: efficient synthesis of xyloolligosaccharides from α-D-xylopyranosyl fluoride through a conjugated reaction, Chembiochem. 23 (2007) 2145–2151.
[12] S. Shulami, G. Zaide, G. Zolotnisky, Y. Langut, G. Feld, A.L. Sonenshein, Y. Shoham, A two-component system regulates the expression of an ABC transporter for xylo-oligosaccharides in *Geobacillus stearothermophilus*, Appl. Environ. Microbiol. 73 (2007) 874–884.
[13] T. Barvman, A. Mechely, S. Shulami, V. Belakhov, T. Baasov, G. Shoham, Y. Shoham, Glutamic acid 160 is the acid-base catalyst of beta-xylosidase from *Bacillus stearothermophilus* T-6: a family 39 glycoside hydrolase, FEBS Lett. 495 (2001) 115–119.
[14] M. Czjzek, A. Ben-David, T. Bravman, G. Shoham, B. Henrissat, Y. Shoham, Enzyme-substrate complex structures of a GH39 beta-xylosidase from *Geobacillus stearothermophilus*, J. Mol. Biol. 353 (2005) 838–846.
[15] T. Bravman, G. Zolotnitsky, V. Belakhov, G. Shoham, B. Henrissat, T. Baasov, Y. Shoham, Detailed kinetic analysis of a family 52 glycoside hydrolase: a β-xylosidase from *Bacillus stearothermophilus*, Biochemistry 42 (2003) 10528–10536.
[16] D. Quintero, Z. Velasco, E. Hurtado-Gómez, J.L. Neira, L.M. Contreras, Isolation and characterization of a thermostable β-xylosidase in the thermophilic bacterium *Geobacillus pallidus*, Biochim. Biophys. Acta 1174 (2007) 510–518.
[17] C.N. Pace, Determination and analysis of urea and guanidine hydrochloride denaturation curves, Methods Enzymol. 131 (1986) 266–280.
[18] S. Martínez-Rodríguez, L. González-Ramírez, J.M. Clemente-Jiménez, F. Rodríguez-Vico, F.J. Las Heras-Vazquez, J.A. Gavira, J.M. García-Ruiz, Crystallization and preliminary crystallographic studies of the recombinant dihydropyrimidinase from *Sinorhizobium meliloti* CECT4114, Acta. Cryst. F. 62 (2006) 1223–1226.
[19] T. Baba, R. Shinke, T. Nanmori, Identification and characterization of clustered genes for thermostable xylan-degrading enzymes, beta-xylosidase and xylanase of *Bacillus stearothermophilus* 21, Appl. Environ. Microbiol. 60 (1994) 2252–2258.
[20] B. Miroux, J.E. Walker, Over-production of proteins in *Escherichia coli*: mutant hosts that allow synthesis of some membrane proteins and globular proteins at high levels, J. Mol. Biol. 260 (1996) 289–298.
[21] C.N. Pace, J.M. Scholtz, Measuring the conformational stability of a protein, in: T.E. Creighton (Ed.), Protein Structure, 2nd ed., Oxford University Press, Oxford, 1997, pp. 253–259.
[22] T. Bravman, G. Zolotnitsky, S. Shulami, V. Belakhov, D. Solomon, T. Baasov, G. Shoham, Y. Shoham, Stereochemistry of family 52 glycosyl hydrolases: a β-xylosidase from *Bacillus stearothermophilus* T-6 is a retaining enzyme, FEBS Lett. 495 (2001) 39–43.
[23] P.W. Atkins, J. de Paula, Physical Chemistry, 8th ed. Oxford University Press, Oxford, 2006.
[24] A.R. Fersht, Structure and mechanism in protein science: a guide to enzyme catalysis and protein folding, W. H. Freeman, New York, 1999.
[25] A. Hinkle, A. Goranson, C. A Butters, L.S. Tobacman, Roles for the troponin tail domain in thin filament assembly and regulation. A deletional study of cardiac troponin T, J. Biol. Chem. 274 (1999) 7157–7164.
[26] A.F. Carvalho, J. Costa-Rodrigues, I. Correia, J.C. Pessoa, T.Q. Faria, C.L. Martins, M. Fransen, C. Sá-Miaranda, J.E. Azevedo, The N-terminal half of the peroxisomal cycling receptor Pex5p is a natively unfolded domain, J. Mol. Biol. 356 (2006) 864–875.
[27] P.J. Darlin, J.M. Holt, G.K. Ackers, Coupled energetics of lambda cro repressor self-assembly and site-specific DNA operator binding I: analysis of cro dimerization from nanomolar to micromolar concentrations, Biochemistry 39 (2000) 11500–11507.
[28] M.I. Muro-Pastor, F.N. Barrera, J.C. Reyes, F.J. Florencio, J.L. Neira, The inactivating factor of glutamine synthetase, IF7, is a "natively unfolded" protein, Protein Sci. 12 (2003) 1443–1454.
[29] P.W. Riddless, R.L. Blakeley, B. Zerner, Reassessment of Ellman's reagent, Methods. Enzymol. 91 (1983) 49–60.
[30] A.P. Minton, Modern Analytical Ultracentrifugation, Birkhauser Boston Inc., Cambridge, MA, Cambridge, MA, 1994.
[31] P. Schuck, Size-distribution analysis of macromolecules by sedimentation velocity ultracentrifugation and Lamm equation modelling, Biophys. J. 78 (2000) 1606–1619.
[32] T.M.S. Laue, T.M. Ridgeway, S.L. Pelletier, Computer-aided interpretation of analytical sedimentation data for proteins, Royal Society of Chemistry, Cambridge, UK, 1992.
[33] F.X. Schmid, Optical spectroscopy to characterize protein conformation and conformational changes, in: T.E. Creighton (Ed.), Protein Structure, 2nd ed., Oxford University Press, Oxford, 1997, pp. 261–297.
[34] G. Bohm, R. Muhr, R. Jaecnicke, Quantitative analysis of protein far UV circular dichroism spectra by neural networks, Protein. Engineering. 5 (1992) 191–195.
[35] C.A. Royer, Fluorescence spectroscopy, in: B.A. Shirley (Ed.), Protein Stability and Folding. Humana Press, Towota, New Jersey, 1995, pp. 65–89.
[36] E. Deu, J.F. Kirsch, Cofactor directed reversible denaturation pathways: the cofactor stabilized *Escherichia coli* aspartate aminotransferase homodimer unfolds through a pathway that differs from that of the apoenzyme, Biochemistry 46 (2007) 5819–5829.
[37] J. Backmann, G. Schäfer, L. Wyns, H. Bönisch, Thermodynamics and kinetics of unfolding of the thermostable trimeric adenylate kinase from the archeon *Sulfolobus acidocaldarius*, J. Mol. Biol. 284 (1998) 817–833.
[38] I. Echabe, J.A. Encinar, J.L.R. Arrondo, Removal of spectral noise in the quantitation of protein structure through infrared band decomposition, Biospectroscopy 3 (1997) 469–475.
[39] I. Smaali, C. Rémond, M.J. O'Donohue, Expression in *Escherichia coli* and characterization of β-xylosidases GH39 and GH-43 from *Bacillus halodurans* C-125, Appl. Microbiol. Biotechnol. 73 (2006) 582–590.
[40] Y.F. Hershcovitz, R. Gilboa, V. Reiland, G. Shoham, Y. Shoham, Catalytic mechanism of SGAP, a double-zinc aminopeptidase from *Streptomyces griseus*, FEBS J. 274 (2007) 3864–3876.
[41] Y. Xue, W. Shao, Expression and characterization of a thermostable β-xylosidase from the hyperthermophile, *Thermotoga maritime*, Bioctechnol. Lett. 26 (2004) 1511–1515.
[42] H. Lumry, H. Eyring, Conformation changes in proteins, J. Phys. Chem. 58 (1954) 110–120.
[43] M.D. Gouda, S.A. Singh, A.G. Appu Rao, M.S. Thakur, N.G. Karanth, Thermal inactivation of glucose oxidase. Mechanism and stabilization using additives, J. Biol. Chem. 278 (2003) 24324–24333.
[44] M.Y. Jeong, S. Kim, C.W. Yun, Y.J. Choi, S.G. Cho, Engineering a *de novo* internal disulfide bridge to improve the thermal stability of xylanase from *Bacillus stearothermophilus* N0. 236, J. Biotechnol. 127 (2007) 300–309.
[45] S. D'amico, J.C. Marx, C. Gerday, G. Feller, Activity-stability relationships in extremophilic enzymes, J. Biol. Chem. 278 (2003) 7891–7896.
[46] T. Suzuki, E. Kitagawa, F. Sakakibara, K. Ibata, K. Usui, K. Kawai, Cloning, expression, and characterization of a family 52 β-xylosidase gene (xysB) of a multiple-xylanase-producing bacterium, *Aeromonas caviae* ME-1, Biosci. Biotechnol. Biochem. 65 (2001) 487–494.
[47] T. Nanmori, T. Watanabe, R. Shinke, A. Kohno, Y. Kawamura Y, Purification and properties of thermostable xylanase and b-xylosidase produced by a newly isolated *Bacillus stearothermophilus* strain, J. Bacteriol. 172 (1990) 6669–6672.
[48] M. Czjek, T. Bravman, B. Henrissat, Y. Shoham, Crystalization and preliminary crystallographic analysis of a thermostable family 52 β-D-xylosidase from *Geobacillus stearothermophilus* T-6, Acta Crystallog. D. 60 (2004) 1461–1463.
[49] G. Zolotnitsky, U. Cogan, N. Adir, V. Solomon, G. Shoham, Y. Shoham, Mapping glucoside hydrolase substrate subsites by isothermal titration calorimetry, Proc. Natl. Acad. Sci. USA 101 (2004) 11275–11280.
[50] T.E. Creighton, Proteins. Structures and macromolecular properties, 2nd. W. H. Freeman, New York, 1993.

[51] R.W. Woody, Circular dichroism, Methods Enzymol. 246 (1995) 34–71.
[52] S.M. Kelly, N.C. Price, The use of circular dichroism in the investigation of protein structure and function, Curr. Prot. and Peptide Sci. 1 (2000) 349–384.
[53] S. Vuilleumier, J. Sancho, R. Loewenthal, A.R. Fersht, Circular dichroism studies of barnase and its mutants: characterization of the contribution of aromatic side chains, Biochemistry 32 (1993) 10303–10313.
[54] A. Barth, S.R. Martin, P.M. Bayley, Resolution of Trp near UV CD spectra of calmodulin-domain peptide complexes into the ^1L_a and ^1L_b component spectra, Biopolymers 45 (1998) 493–501.
[55] R.L. Thurlkill, G.R. Grimsley, J.M. Scholtz, C.N. Pace, p*K* values of the ionizable groups of proteins, Protein Sci. 15 (2006) 1214–1218.
[56] G.V. Semisotnov, N.A. Rodionova, O.I. Razgulyaev, V.N. Uversky, A.F. Gripas, R.I. Gilmanshin, Study of the "molten globule" intermediate state in protein folding by a hydrophobic fluorescent probe, Biopolymers 31 (1991) 119–128.
[57] F. Conejero-Lara, P.L. Mateo, F.X. Aviles, J.M. Sánchez-Ruiz, Effect of Zn^{2+}on the thermal denaturation of carboxypeptidase B, Biochemistry 30 (1991) 2067–2072.
[58] M.L. Galisteo, P.L. Mateo, J.M. Sánchez-Ruiz, Kinetic study on the irreversible thermal denaturation of yeast phosphoglycerate kinase, Biochemistry 30 (1991) 2061–2066.
[59] J.M. Sánchez-Ruiz, J.L. López-Lacomba, M. Cortijo, P.L. Mateo, Differential scanning calorimetry of the irreversible thermal denaturation of thermolysin, Biochemistry 27 (1988) 1648–1652.
[60] K. Imada, M. Sato, N. Tanaka, Y. Katsube, Y. Matsuura, T. Oshima, Three dimensional structure of a highly thermostable enzyme, 3-isopropylamalate deshydrogenase of *Thermus thermophilus* at 2.2 Å resolution, J. Mol. Biol. 222 (1991) 725–728.
[61] S.E. Jackson, How do small single-domain proteins fold? Folding and Des. 3 (1998) R81–R91.
[62] R. Jaenicke, H. Lilie, Folding and association of oligomeric and multimeric proteins, Adv. Protein Chem. 53 (2000) 329–401.
[63] J. Fitter, J.R. Herrmann, N.A. Dencher, A. Bume, T. Hauss, Activity and stability of a thermostable alpha-amylase compared to its mesophilic homologue: mechanisms of thermal adaptation, Biochemistry 40 (2001) 10723–10731.
[64] T. Bravman, V. Belakhov, D. Solomon, G. Shoham, B. Henrissat, T. Baasov, Y. Shoham, Identification of the catalytic residues in family 52 glycoside hydrolase, a β-xylosidase from *Geobacillus stearothermophilus* T-6, J. Biol. Chem. 278 (2003) 26742–26749.
[65] M. Weijers, P.A. Barnevel, M.A. Cohen Stuart, R.W. Visschers, Heat-induced denaturation and aggregation of ovalbumin at neutral pH described by irreversible first-order kinetics, Protein Sci. 12 (2003) 2693–2703.
[66] C. Duy, J. Fitter, Thermostability of irreversible unfolding alpha-amylases analyzed by unfolding kinetics, J. Biol. Chem. 280 (2005) 37360–37365.
[67] S. Chakravarty, R. Varadarajan, Elucidation of determinants of protein stability through genome sequence, FEBS Lett. 470 (2000) 65–69.
[68] N.E. Robinson, A.B. Robinson, Molecular clocks, Proc. Natl. Acad. Sci. USA 98 (2001) 944–949.
[69] J. Kongsted, U. Ryde, J. Wydra, J.J. Jensen, Prediction and rationalization of the pH dependence of the activity and stability of family 11 xylanases, Biochemistry 46 (2007) 13581–13592.
[70] O.B. Ptitsyn, Molten globule and protein folding, Adv. Protein Chem. 47 (1995) 83–229.